Ascent Aeromaneuvering Capabilities of Transatmospheric Vehicles

Gene P. Menees* and Michael E. Tauber*
NASA Ames Research Center, Moffett Field, California
John T. Wilson†
Sterling Software, Palo Alto, California
and
Henry G. Adelman‡
Eloret Institute, Sunnyvale, California

The low-Earth-orbit (LEO) rendezvous capability of a conceptual transatmospheric vehicle is analyzed for two endo-/exoatmospheric ascent missions. Both cases involve coasting aerodynamic maneuvers starting from the burn-out conditions corresponding to airbreathing propulsion systems that achieve orbital velocity within the atmosphere. The powered phase of the ascent trajectories approximate constant dynamic pressure, fuel-efficient flight paths typically flown by supersonic aircraft. The aeromaneuvering coast phases of the ascent include both coplanar (to determine altitude capability without plane-inclination changes) and aeroturning to LEO rendezvous at 400 km altitude (to assess plane-change capability). The coast-phase ascent maneuvers are correlated with G-load requirements and aerothermodynamic heating characteristics at two critical locations on the vehicle surface (i.e., the nose stagnation point and the body centerline). Recommendations are made concerning thermal protection requirements.

Nomenclature

G	= vehicle acceleration normalized by g
g	= acceleration of gravity
H	= altitude
L/D	= lift-to-drag ratio
q	= dynamic pressure
t	= flight time from H_o
V	= flight velocity
V_x, V_y, V_z	= velocity in Cartesian coordinates
x, y, z	= Cartesian coordinates (e.g., x = downstream distance on vehicle centerline from nose)
β	= ballistic coefficient
γ	= flight-path angle relative to local horizon
Δi	= plane-inclination change angle
ΔV	= equivalent propulsive thrust velocity increment
ϕ	= local body angle with respect to freestream

Subscripts

a	= apogee of ascent trajectory
c	= circularization requirement at LEO
e	= atmospheric entry condition
o	= burn-out condition for airbreathing propulsion (start of coast maneuver)
x	= exit condition from sensible atmosphere
γ	= relative change with flight-path angle

Introduction

THE developing need for economical access to space and transoceanic transportation has produced a resurgence in the demand for hypervelocity, transatmospheric vehicles (TAV's). This new class of aerospace vehicles would have flexible and responsive operational characteristics approaching those of aircraft and would eventually replace the Space Shuttle by providing short launch notice and turnaround times. A TAV would have the capability to take off and land from ordinary runways and operate in low-Earth-orbits (LEO). These vehicles can play crucial roles in supporting the future space station program and maintaining the nation's lead role in global civil transportation.

Preliminary studies have indicated that high-altitude aerodynamic maneuvering capability not only enhances mission options but is potentially important for long-distance efficiency in future hypervelocity transportation vehicles. The historical technology base for hypersonic cruise and Earth to LEO airbreathing vehicles was developed between the early 1950s and 1970s. After this period, research efforts decreased to a low level because of the nation's commitment to the rocket-powered, Space Shuttle transportation system. A representative sampling of the previous work is given in Refs. 1-7, and a commendable summary appears in Ref. 8. None of the prior work provided in-depth mission analysis studies that exploited transatmospheric aeromaneuvering capabilities. The present effort emphasizes this important area, with the initial phase containing a parametric analysis of the LEO rendezvous capability of a conceptual TAV for coplanar and aeroturning endo-/exoatmospheric ascent missions (Fig. 1). Future work will include the development of exo-/endoatmospheric aeromaneuvering mission requirements involving multiple transatmospheric passes and descent to a horizontal landing.

Aerodynamic Characteristics

Estimates of the high-altitude, hypersonic aerodynamic characteristics of the vehicle for the principal parameter required in this study, lift-to-drag ratio, are given in Fig. 2. The results are representative of the requirements for a low-drag TAV that can achieve orbital velocity within the atmosphere using advanced airbreathing propulsion systems. The deterioration of the lifting capability in the rarefied flight regimes of the outer atmosphere is also included in Fig. 2.

Presented as Paper 87-0513 at the AIAA 25th Aerospace Sciences Meeting, Reno, NV, Jan. 12-15, 1987; received Jan. 26, 1987; revision received June 20, 1987.

*Research Scientist. Associate Fellow AIAA.
†Consultant, Professional Services Operations West.
‡Research Scientist. Member AIAA.

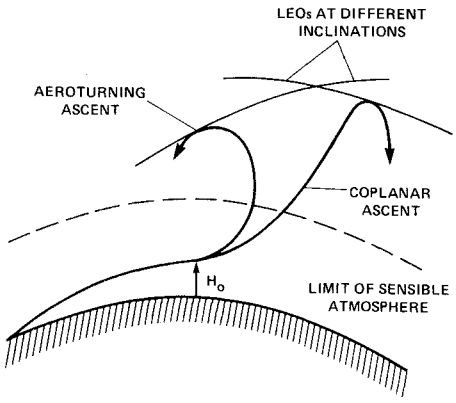

Fig. 1 Candidate ascent to LEO aeromaneuvering missions.

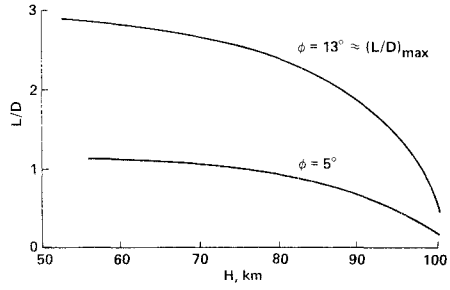

Fig. 2 Estimated hypersonic aerodynamic characteristics including low-density viscous effects.

These results were obtained by correlation with previous work[9] on high-lift aeroassisted orbital transfer vehicles that accounted for hypervelocity, low-density viscous phenomena on the aerodynamic forces.

Trajectory Analysis

Trajectory Program

The research tool employed by this paper is our long-used computer program WTRAJ, which was developed at NASA Ames by J. F. Wilson. This custom-made program is straightforward, fast, and accurate for our purposes. Its focus is near-planet trajectories, including both outside the atmosphere orbits and inside the atmosphere aerotransits. The program numerically integrates Newton's equations of motion (e.g., see Ref. 10 for analytical details); a predictor-corrector numerical scheme is used; time is the independent variable. The geometry is fully three-dimensional with a rotating planet (the atmosphere's rotational speed is a function of latitude). The integration proceeds in the inertial coordinate system. The vehicle's state vector is, at all times, calculated in both inertial coordinates (x, y, z, V_x, V_y, V_z) and astrodynamic coordinates (radius, latitude, longitude, speed, flight angle, azimuth). The air-relative speed is also calculated, and all orbital elements (semimajor length, eccentricity, inclination, longitude of ascending node, longitude of periapsis, true anomaly) are also calculated at all times. The program can account for the perturbations due to the planet's oblateness and due to a single moon's effect; however, since the trajectories of this study are of low altitude and short duration, this paper neglects these perturbations. The aerodynamic forces of drag and lift are included in the program; the lift vector may be rolled down from the vertical to produce a lateral (turning) force; also the roll may be controlled (automatically) to produce a glide trajectory (constant flight angle). The atmosphere model is a table of density vs altitude, which for Earth is based on the U.S. Standard Atmosphere, 1962. The thrust force is also included, along with the pitch angle of the thrust vector. Thrust may be applied either outside or inside the atmosphere. The vehicle's mass decreases as the thrusting consumes propellant (at a rate determined by the input specific impulse of the engine—rocket or airbreathing) and, at each time, the net of all force vectors felt by the passenger (the G load) is calculated.

Starting Conditions

The analysis starts at the burn-out conditions for altitude (H_o) and velocity (V_o) previously analyzed[11] for airbreathing propulsion systems that achieve orbital velocity (8 km/s) within the atmosphere. The powered-ascent flight paths allow conditions to be varied parametrically over a broad range. The paths approximate constant dynamic pressure, fuel-efficient trajectories typically flown by supersonic aircraft. The coasting-ascent capability for LEO rendezvous is developed from the burn-out conditions for constant q trajectories of 0.1 and 0.4 atm. The two cases illustrated in Fig. 1 are in the coast phase of the ascent, including 1) coplanar to determine altitude capability exclusive of plane-inclination changes, and 2) aeroturning to LEO rendezvous at 400 km altitude to assess aeromaneuvering plane-change capability. Throughout this study, the vehicle's lift is increased instantaneously over that of the nonlifting case, which initially enhances the aerothermodynamic heating and G loads, as will be shown subsequently. This procedure is probably unrealistic for actual operational scenarios, and guidance and control schemes would be devised to alleviate the application of lift. However, such refinements require design details that are beyond the scope of this study.

Flight Parameters

The key flight parameters that determine the LEO rendezvous capability, or apogee altitude of the coasting-ascent trajectory, are L/D, β, γ, and ϕ. The influence of lift-to-drag ratio (L/D) on H is evaluated by considering both lifting and nonlifting cases for each of the constant q powered-ascent trajectories. The maximum L/D ($\phi \approx 13$ deg, Fig. 2) is applied in the trajectory equations for all lifting calculations with $\beta = 500$ kg/m^2 to achieve maximum apogee altitude capability. For the nonlifting cases ($\phi = 0$ deg), β is set equal to 1000 kg/m^2 to account for the decrease in drag coefficient and frontal area.

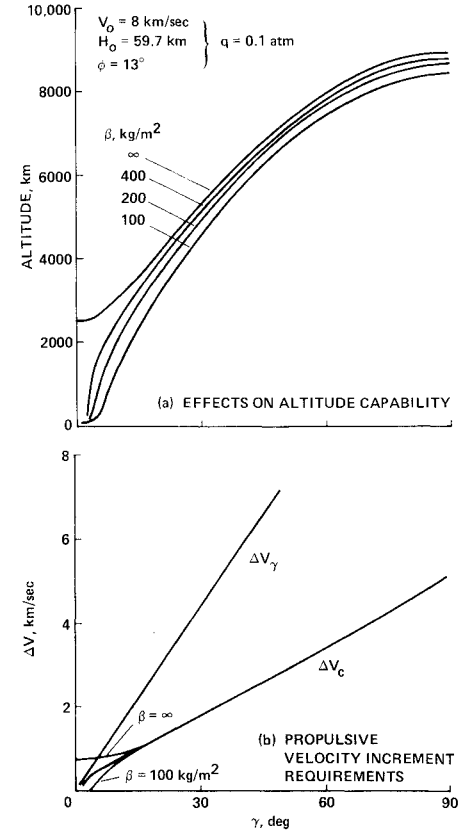

Fig. 3 Effect of key flight parameters (β, γ) on coplanar LEO rendezvous capability.

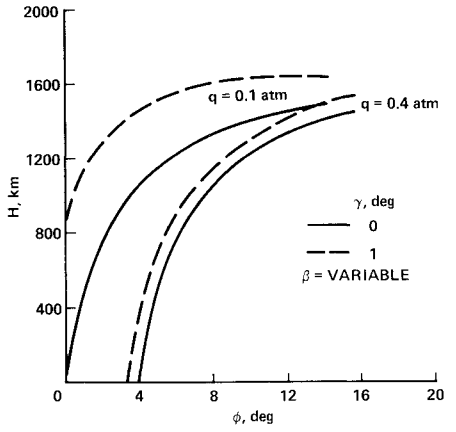

Fig. 4 Effect of incidence and flight-path angles on coplanar LEO rendezvous altitude.

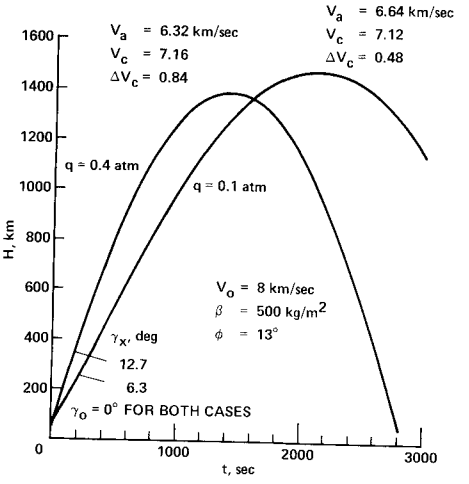

Fig. 5 Effect of constant dynamic pressure ascent trajectories on coplanar LEO rendezvous.

Coplanar Ascent

Details of the effects of β, γ, and ϕ on H are illustrated in Figs. 3–5 for the $q = 0.1$ atm ascent trajectory. Results for broad variations in γ and β are shown in Fig. 3. Major changes in altitude capability are produced by γ (Fig. 3a), but the effect tends to diminish and level off as high values are approached near 90 deg. The significant effects of β occur over a relatively low range of values for γ (≤ 10 deg), because of the decreasing impact of the vehicle weight vector resulting from high flight-path angles. The propellant sacrificed because of changes in γ and β is indicated in Fig. 3b by the equivalent propulsive thrust velocity increments ΔV_γ and ΔV_c, respectively. Large penalties are incurred with increasing γ, indicating that low flight-path angles are necessary to maximize vehicle performance. The impact of ϕ on LEO altitude is shown in Fig. 4 for both constant q trajectories. The lower q achieves a higher altitude, although the coast maneuver starts in the lower-density regime of a higher H, which produces less lift. Conversely, the high q case starts at a lower altitude, which produces more drag as well as lift. The resulting tradeoff in these factors is shown in Fig. 5, in which the details of the flight trajectories, including the atmospheric exit and apogee conditions, are shown as a function of flight time.

The effect of lift on the coasting maneuver is shown in Figs. 6 and 7 for the $q = 0.1$ and 0.4 atm ascent trajectories, respectively. For the $q = 0.1$ atm nonlifting case (Fig. 6a), the vehicle has insufficient kinetic energy to escape the atmosphere until γ exceeds 0.4 deg, but eventually reaches an apogee altitude for LEO rendezvous near 850 km for $\gamma = 1.0$ deg. The effect of lift shown in Figs. 6a and 6b is, however, dramatic and propels the vehicle out of the atmosphere to much higher altitudes than the nonlifting case. An altitude of more than 1600 km is achieved for the high-lift case (Fig. 6c), even for $\gamma = 0$ deg. Similar results were obtained for the $q = 0.4$ atm case shown in Fig. 7, except that lower LEO altitudes are obtained and the value of γ necessary to leave the atmosphere increases by almost an order of magnitude. This occurs because of the longer duration of high-drag flight at lower altitudes, which is characteristic of the high-q ascent trajectory. It should also be noted that values for the equivalent propulsive-thrust velocity increments, ΔV_γ and ΔV_c, required for flight-path changes and LEO circularization are given in Figs. 6 and 7.

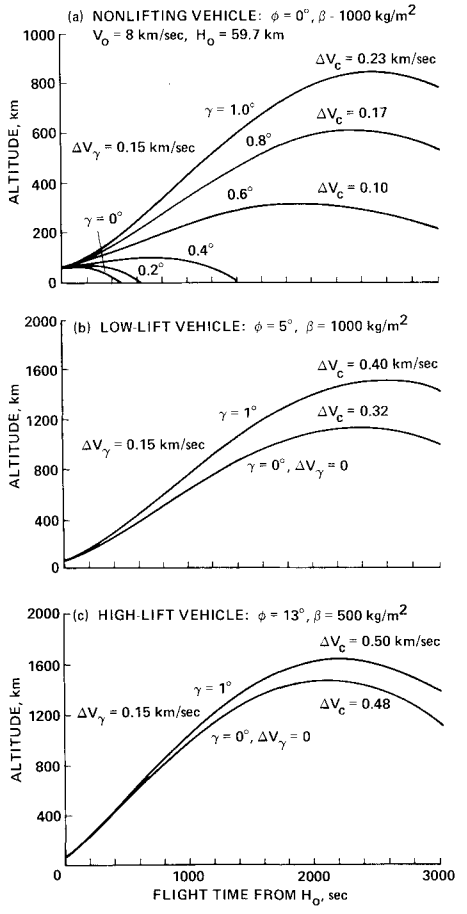

Fig. 6 Coplanar LEO rendezvous capability for $q = 0.1$ atm ascent trajectory.

Aeroturning Ascent

The capability of the vehicle to produce plane-inclination changes and the resulting consequences to the propulsion requirements are illustrated in Fig. 8. The key flight parameter for this maneuver is γ, since β and ϕ are fixed at values corresponding to the maximum obtainable L/D. Figure 8a shows that the aeroturning ability increases with negative values of γ, which occurs because the vehicle remains in the atmosphere longer than for positive γ. However, the price paid for the negative γ flight strategy is a larger propellant penalty for ΔV_c, since ΔV_γ is unaffected by the sign of γ (Figs. 8b and 8c). The results show that the plane-change capability ($\Delta i = 23$ deg) is fairly substantial for the $q = 0.4$ atm trajectory and $\gamma = -3$ deg. The propellant penalties incurred for ΔV_c and ΔV_γ for these flight conditions are generally acceptable, considering contemporary specific-impulse goals for rocket engines (i.e., 480 s).

Aerothermodynamic Heating

An essential aspect of this work is the heating analysis at critical locations on the vehicle surface. Because of the extended periods of hypervelocity flight required to attain

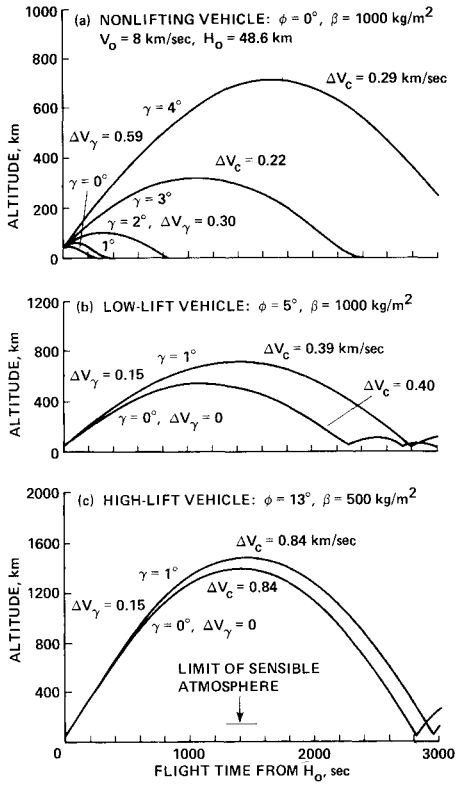

Fig. 7 Coplanar LEO rendezvous capability for $q = 0.4$ atm ascent trajectory.

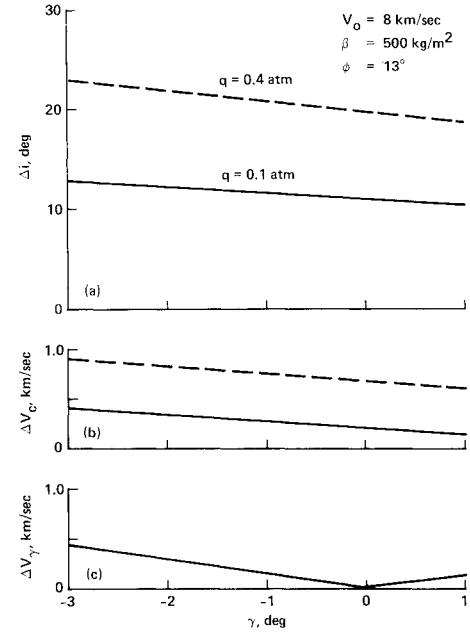

Fig. 8 Effect of γ on aeroturning capability to LEO rendezvous at 400 km: a) plane-inclination change; b) ΔV_c requirements for tangential circularization; c) ΔV_γ requirements.

orbital velocity within the atmosphere using an airbreathing propulsion system, the vehicle will be subjected to long periods of high heat fluxes and heating loads. These conditions determine the thermal-protection requirements and, therefore, define limitations on the mission capability of the vehicle. The analytical methods used to predict the heating characteristics were developed and reported previously.[11] The same techniques are applied in the present study for the aeromaneuvering ascent missions. Results for the total heat loads are combined with those of the powered phase of the ascent trajectories for completeness in the analysis of thermal-protection requirements.

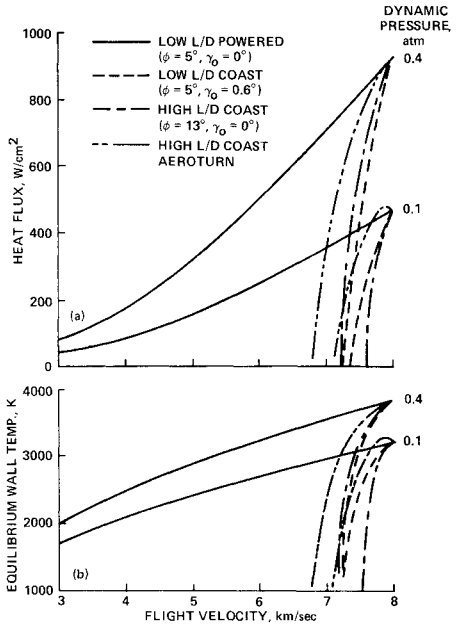

Fig. 9 Ascent heating at stagnation point for 10-cm nose radius: a) heat flux; b) equilibrium wall temperature.

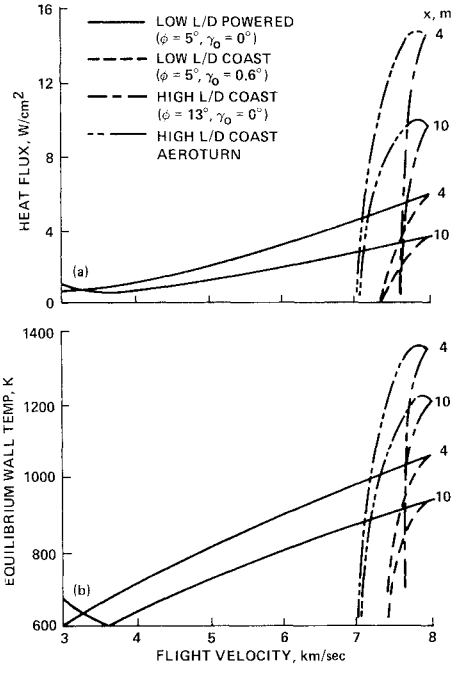

Fig. 10 Ascent heating at body centerline for dynamic pressure = 0.1 atm trajectory: a) heat flux; b) equilibrium wall temperature.

The predicted ascent heating rates and equivalent equilibrium wall temperatures at the vehicle stagnation point are given in Fig. 9 as a function of flight velocity. The previous powered-phase results are represented by the solid curves, whereas the present coast-phase calculations are shown by the broken curves. As expected, the magnitudes of both quantities decrease rapidly from the peak values for all of the coast maneuvers as the vehicle decelerates from the burn-out velocity of 8 km/s.

Centerline heating distributions at streamwise locations of $x = 4$ and 10 m are shown in Figs. 10 and 11 for the $q = 0.1$ and 0.4 atm cases, respectively. The significant point in these two figures is that the heating is greatly enhanced for the high-lift cases, which is produced by the higher incidence of the vehicle. In fact, transition to turbulent flow is produced at $x = 10$ m for the lower-starting, higher-density altitude of the $q = 0.4$ atm trajectory. The heating is increased by almost a

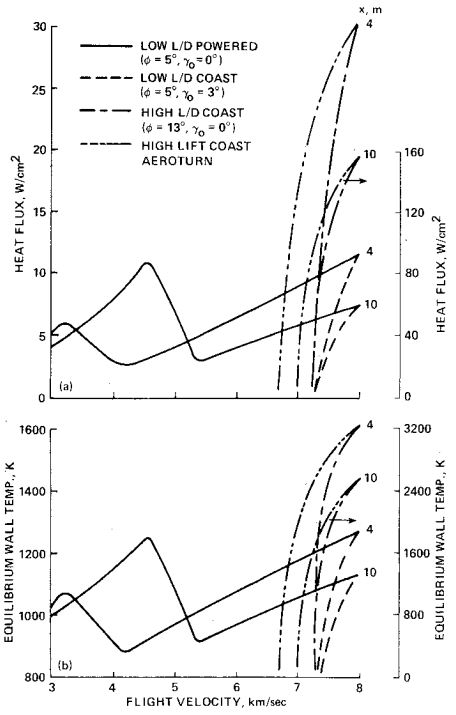

Fig. 11 Ascent heating at body centerline for dynamic pressure = 0.4 atm trajectory: a) heat flux; b) equilibrium wall temperature.

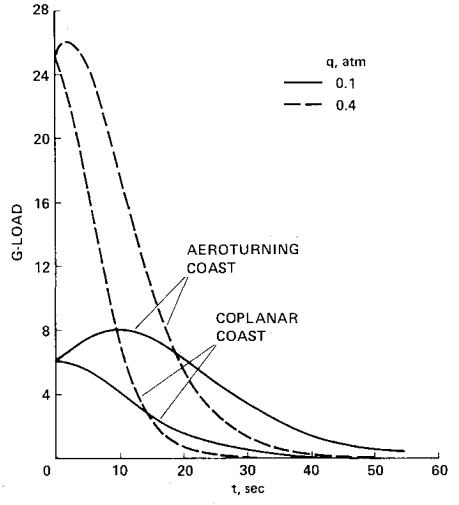

Fig. 12 G-load characteristics for coplanar and aeroturning coasting-ascent maneuvers.

factor of 20 over that for the low L/D case, which occurs because of both turbulence and the higher incidence. The corresponding surface temperature is increased to about 2500 K, which is well beyond the range of reusable materials, making active cooling imperative for this region of the vehicle. On the forward part of the vehicle, however, the wall temperature stays below 1600 K, which is still within the range of current reusable materials technology.

All of the foregoing phenomena result from the instantaneous application of the vehicle's lift, which may not occur in actual flight situations, as discussed previously. In addition, the contribution of the coast-phase heating rates to the total heat loads is not shown herein, since the magnitude is only about 10% of the previous results for the powered phase of the ascent.[11]

Deceleration Loads

The G-load characteristics of the vehicle are crucial to the manned rating, structural design requirements, and, therefore, the mission capability. Human tolerance to G loads varies greatly depending upon physical conditioning and the functional design features of the vehicle, such as position and support. For example, commercial aircraft pull less than 1.2 g, the Shuttle about 1.6 g, fighter aircraft about 7 g, and well-supported astronauts have been subjected to 8–10 g. Without qualification, high-G loads mean severe structural problems and increased vehicle weights with corresponding penalties in mission capability. Consequently, TAV missions must be designed with acceptable compromises in the G-load capability and thermal-protection requirements. For the present study, the G loads did not exceed 1.7 g for the range of accelerations specified during the powered phase of the ascent. Results are given in Fig. 12 for the $q = 0.1$ and 0.4 atm trajectories, respectively. These results involve the lifting vehicle with the lift applied instantaneously at burn-out. The G loads are, therefore, highest during the coast phase of the ascent, ranging from a maximum value of 8 g for $q = 0.1$ atm to 26 g for $q = 0.4$ atm. The magnitude of the G loads should be decreased substantially by gradually increasing the incidence, as the vehicle coasts to the lower-density regions of the atmosphere.

Concluding Remarks

The results of this preliminary exploratory study indicate that the conceptual transatmospheric vehicle design has significant low-Earth-orbit rendezvous capability. Altitudes on the order of 300 km (e.g., Shuttle rendezvous or a future space station) are easily reached and values around 1600 km should be attained without difficulty. In addition, the aerodynamic plane-change capability may be substantial with constant dynamic pressure powered-ascent trajectories that exceed 0.4 atm. The aerothermodynamic heating analysis for the coast phase of the ascent indicates that previous results for the powered phase of the ascent are generally not significantly changed. The exception to this may occur at locations far downstream on the vehicle centerline where turbulent boundary-layer phenomena may cause greatly enhanced heating rates that require active cooling for thermal protection. The magnitude of the G loads for the current aerodynamic lifting maneuver are too severe for man-rating and vehicle design requirements. Alternative flight strategies are being investigated for the implementation of lift after termination of the powered ascent. Future work will also include the investigation of higher constant dynamic pressure powered-ascent trajectories (i.e., >0.5 atm).

References

[1]Eggers Jr., A. J., Allen, H. J., and Neice, S. E., "A Comparative Analysis of the Performance of Long-Range Hypervelocity Vehicles," NACA Rept. 1382, 1958.

[2]Stollery, J. L., "Towards the Ballistic Airliner," *Discovery*, April 1962, pp. 9–17.

[3]Syvertson, C. A., Anderson, J. L., and Kenyon, G. C., "Some Considerations of the Performance of a Maneuverable Lifting-Body Entry Vehicle," AAS Symposium on Space Rendezvous, Rescue, and Recovery, Edwards AFB, CA, Sept. 1963.

[4]Becker, J. B., "Study of High Lift/Drag Ratio Hypersonic Configurations," Fourth Congress of the International Council of the Aeronautical Sciences, Aug. 1964.

[5]Morris, R. E. and Williams, N. B., "A Study of Advanced Airbreathing Launch Vehicles with Cruise Capability," NASA CR-73194 through 73199, 1968.

[6]Love, E. S., "Manned Lifting Entry," *Astronautics & Aeronautics*, Vol. 4, May 1966, pp. 54–64.

[7]Henry, J. R. and McLellan, C. H., "The Airbreathing Launch Vehicle for Earth-Orbit Shuttle—New Technology and Development Approach," AIAA Paper 70-269, Feb. 1970.

[8]Eggers Jr., A. J., Peterson, R. H., and Cohen, N. B., "Hypersonic Aircraft Technology," *Astronautics & Aeronautics*, June 1970, pp. 30–41.

[9]Menees, G. P., "Design and Performance Analysis of an Aeromaneuvering Orbital-Transfer-Vehicle Concept," IAF Preprint 85-139, Stockholm, Sweden, Oct. 1985.

[10]Miele, A., *Flight Mechanics—Theory of Flight Paths*, Vol. 1, Addison-Wesley, New York, 1962.

[11]Tauber, M. E., Menees, G. P., and Adelman, H. G., "Aerothermodynamics of Transatmospheric Vehicles," *Journal of Spacecraft and Rockets*, Vol. 24, No. 9, Sept.-Oct. 1987, pp. 594–602.